

Supplementary Materials for

Therapeutic targeting of metabolic vulnerabilities in cancers with MLL3/4- COMPASS epigenetic regulator mutations

Authors:

Zibo Zhao^{1,2}, Kaixiang Cao^{1,2}, Jun Watanabe^{1,3}, Cassandra N. Philips^{1,2}, Jacob M. Zeidner^{1,2}, Yukitomo Ishi^{1,3}, Qixuan Wang^{1,2}, Sarah R. Gold^{1,2}, Katherine Junkins^{1,2}, Elizabeth T. Bartom^{1,2}, Feng Yue^{1,2}, Navdeep S. Chandel^{1,2,3,4}, Rintaro Hashizume^{1,3}, Issam Ben-Sahra^{1,2}, and Ali Shilatifard^{1,2*}

Affiliations:

¹Department of Biochemistry and Molecular Genetics, Northwestern University Feinberg School of Medicine, 320 E. Superior St., Chicago, IL 60611, USA

²Simpson Querrey Center for Epigenetics, Northwestern University Feinberg School of Medicine, Chicago, IL 60611, USA

³ Robert H. Lurie NCI Comprehensive Cancer Center, Northwestern University Feinberg School of Medicine, Chicago, IL 60611, USA

⁴ Department of Medicine, Northwestern University Feinberg School of Medicine, Chicago, IL 60611, USA

The authors have declared that no conflict of interest exists.

*Correspondence and proofs should be sent to the following address:

Ali Shilatifard

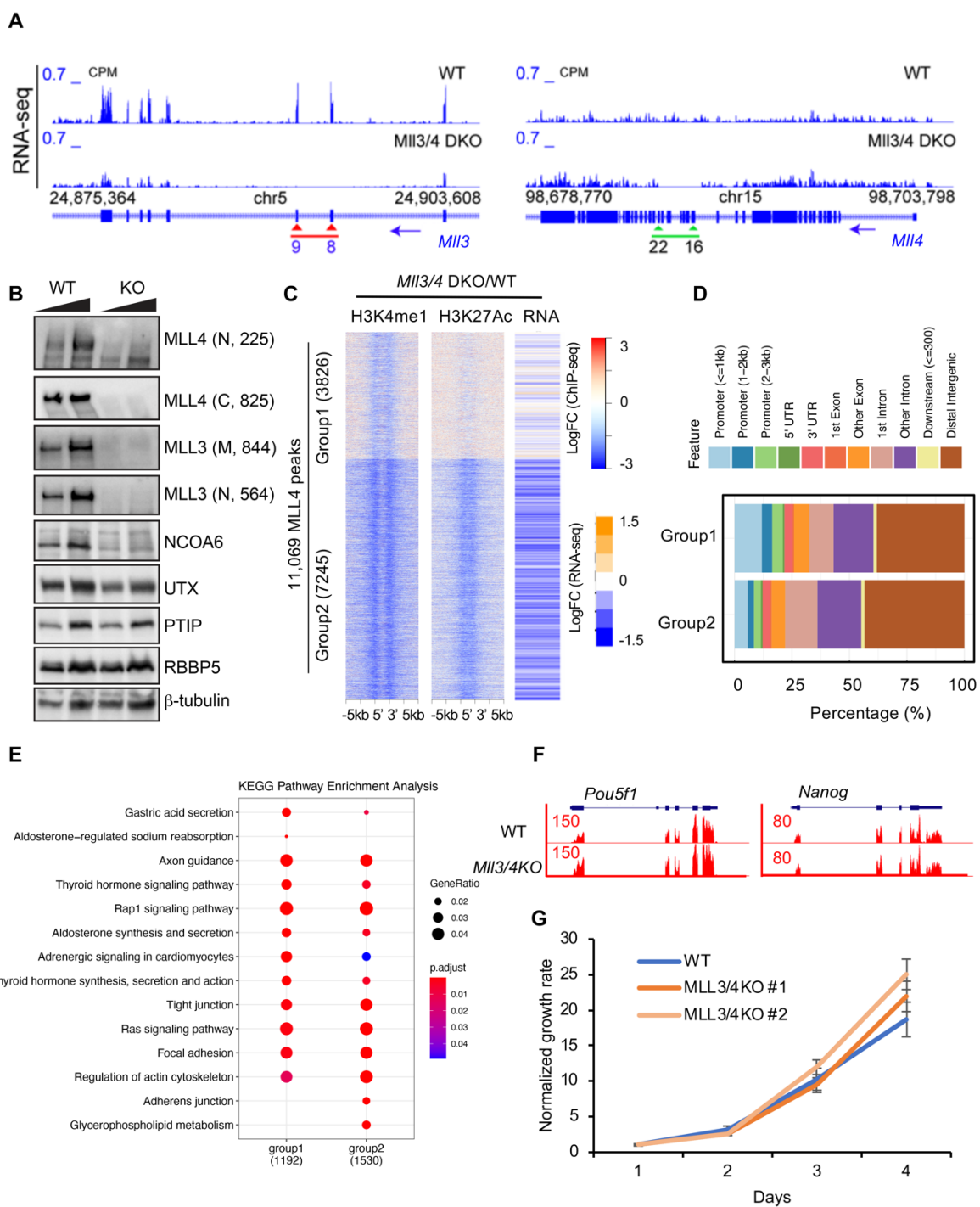
Department of Biochemistry and Molecular Genetics
Northwestern University Feinberg School of Medicine
Simpson Querrey 7th Floor
303 E. Superior St.
Chicago, IL 60611, USA

Email: ASH@northwestern.edu

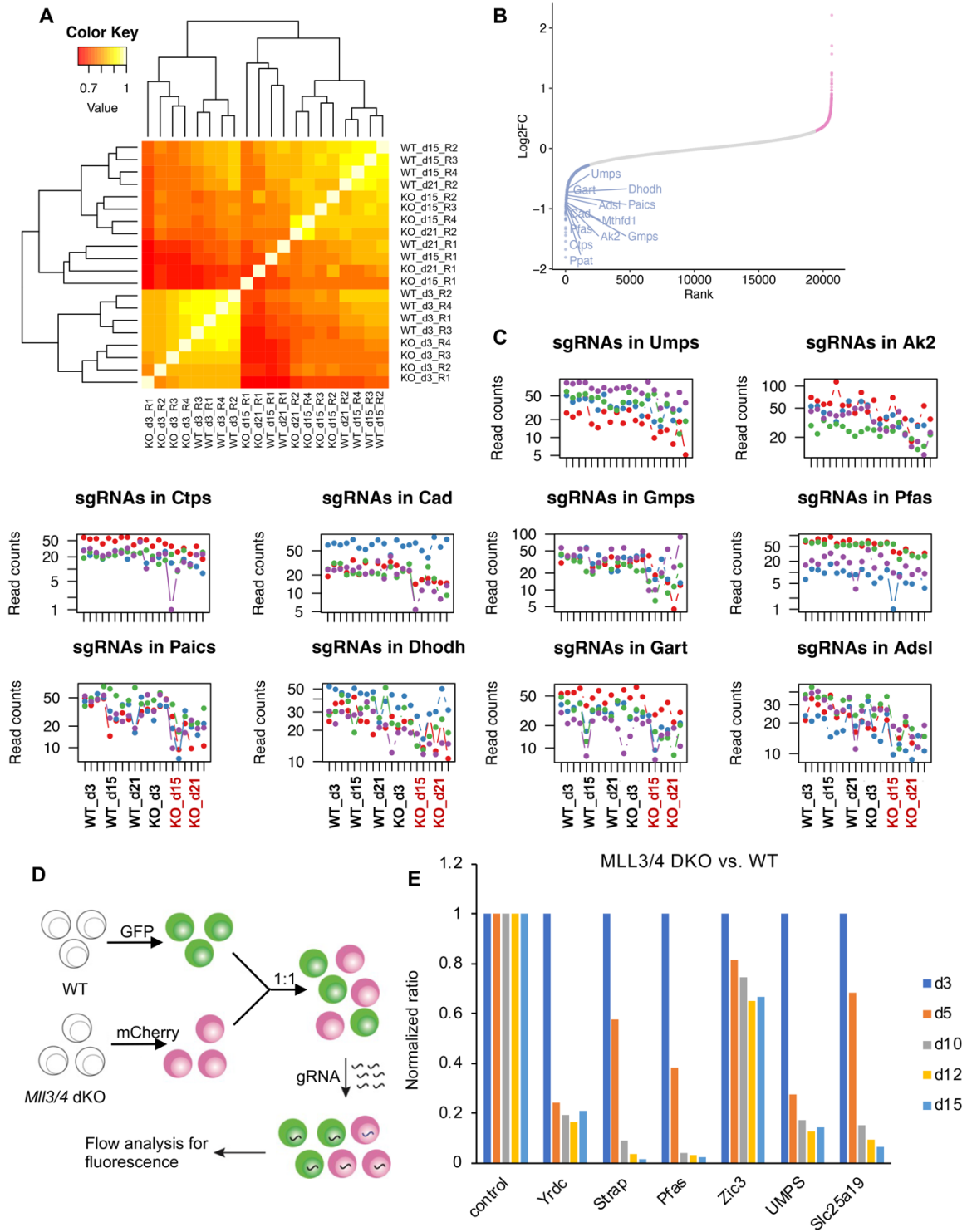
The PDF file includes:

Supplemental Figure 1 to 15

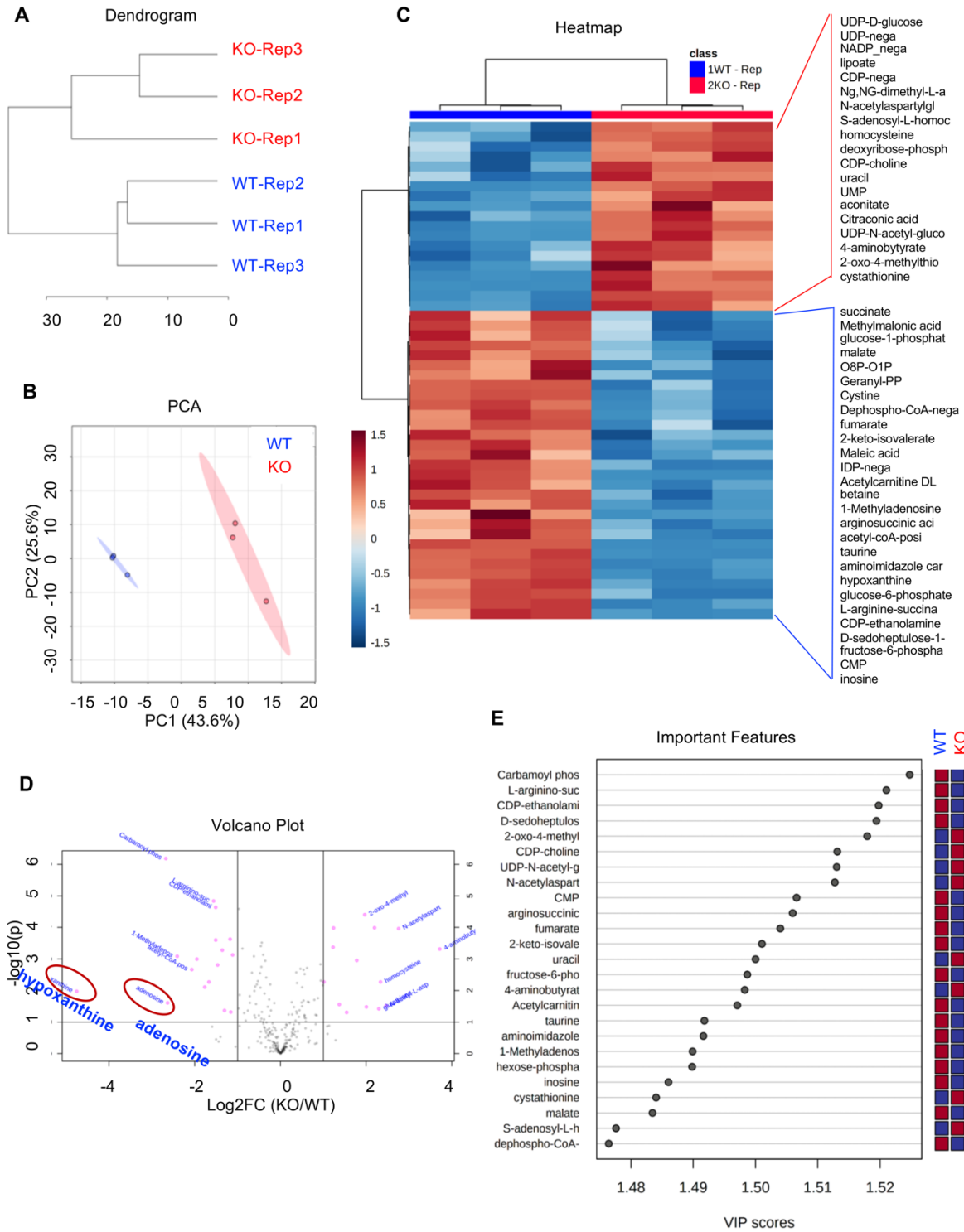
Supplemental Table 1



Supplemental Figure 1. Characterization of MLL3 and MLL4 double knockout mESCs. (A) RNA-seq track showing the CRISPR strategy to knock out MLL3 and MLL4 by targeting exons 8-9 and exons 16-22, respectively. (B) Western blot showing the successful knockout of MLL3 and MLL4 with β -tubulin and the pan-COMPASS subunit RBBP5 as internal controls. Other subunits specific to MLL3/4 COMPASS including NCOA6, UTX, and PTIP are also shown with decreased signals in MLL3/4 KO cells. N, N-terminus; M, middle region; C, C-terminus. (C) H3K4me1 and H3K27Ac ChIP-seq was performed in WT and MLL3/4 KO cells. K-means clustering (k=2) separated the previously defined MLL4 peaks (I) into two groups based on the log2 fold change in H3K4me1 and H3K27Ac ChIP-seq signals. In the meta-analysis shown, H3K4me1 and H3K27Ac reduction coincides with strongly reduced expression of genes at Group2 MLL4 peaks in MLL3/4 KO cells. (D-E) Feature distribution of Group1 and Group2 MLL4 peaks (D) and the KEGG pathway enrichment analysis of Group1 and Group2 genes (E) using the ChIPseeker package(2). (F) RNA-seq track showing the *Pou5f1* and *Nanog* gene expression in WT and MLL3/4 KO cells. (G) Cell growth rates of WT and MLL3/4 KO cells after sustained passaging. Cells were seeded in 6-well plates at 1×10^5 cells/mL. Cell number was counted with Beckman Vi-Cell XR Cell Viability Analyzer. Cell numbers were normalized to day 1. n=2.

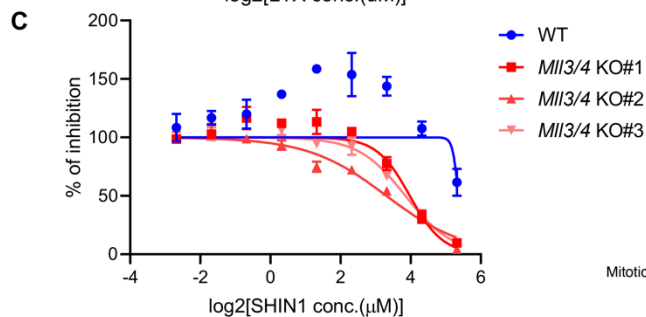
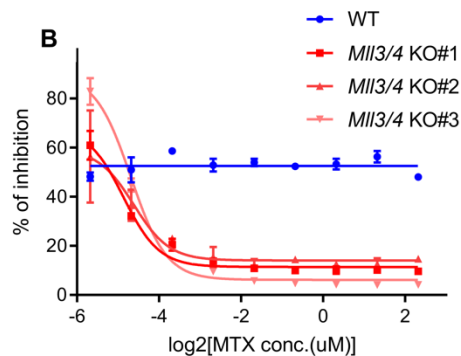
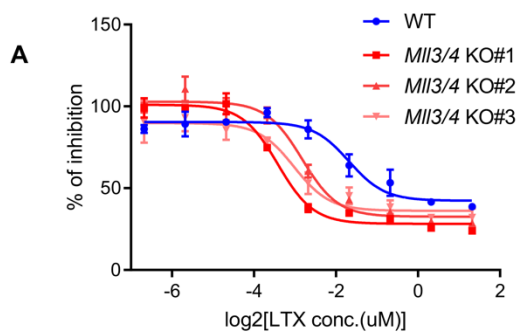


Supplemental Figure 2. Genome-wide Screen Identifies Purine and Pyrimidine Synthesis Pathways as Essential in MLL3/4 KO mESCs. (A) Sample clustering of replicates for different conditions and time points. (B) Overall log₂FC rank plot with purine/pyrimidine genes highlighted. (C) Distribution of sgRNA read counts (normalized) of purine/pyrimidine synthesis genes in WT and KO cells at different time points. (D) WT and KO cells were labeled with GFP and mCherry and were mixed at a 1:1 ratio. Mixed cells were infected with sgRNAs, and fluorescence was analyzed with flow cytometry. (E) The validation of several negatively selected genes in MLL3/4 KO. Normalized ratio of mCherry/GFP indicating selective sgRNA impact on KO cells.

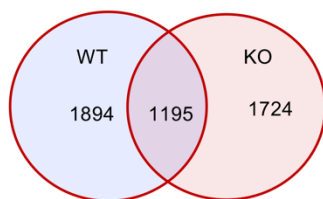


Supplemental Figure 3. Global Steady State Metabolomics of WT and MLL3/4 KO mESCs.

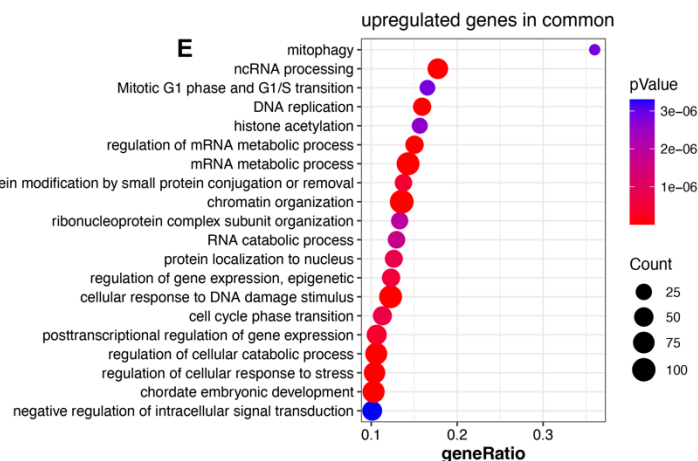
(A) Dendrogram of steady state metabolomics for WT and KO cells. (B) PC analysis of WT and KO cells steady state metabolomics. (C) Hierarchical clustering heatmap showing the differentially abundant metabolites in WT and KO cells. The scale bar represents the Z-score. (D) Volcano plot showing the significantly altered metabolites by log₁₀ p value and log₂ fold change. (E) Important metabolic features in WT and KO cells ranked by VIP scores.



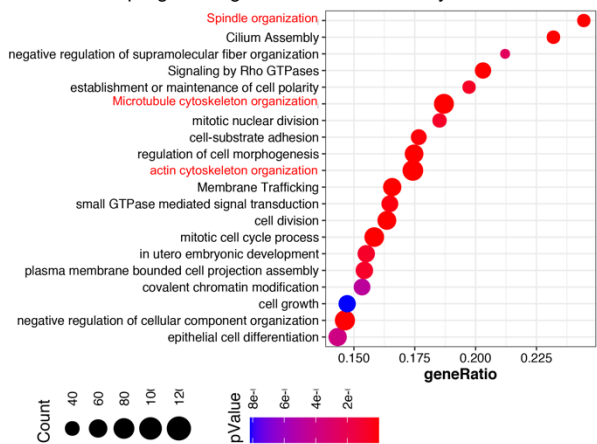
D LTX_vs_DMSO: Up-regulated (adj.p <0.01)



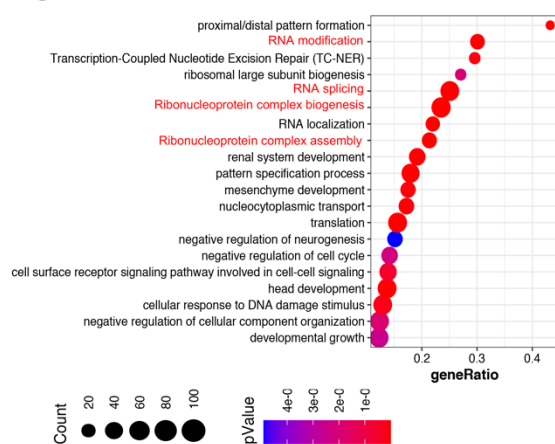
regulation of protein modification by small protein conjugation or removal



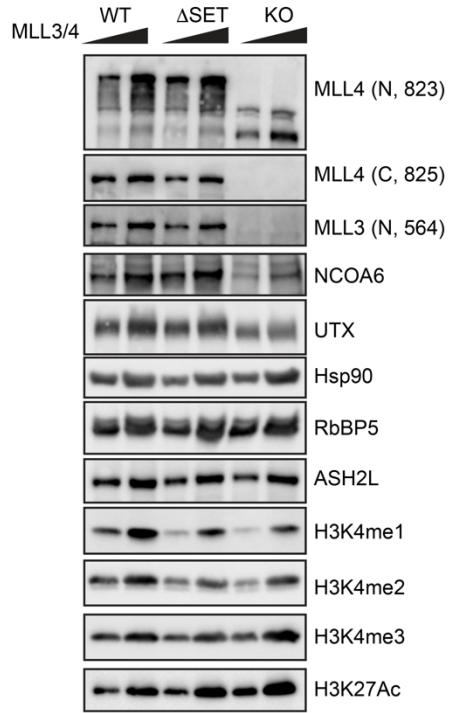
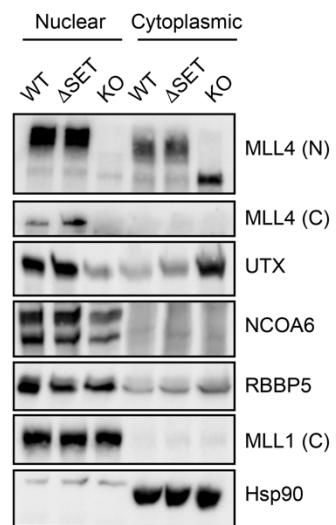
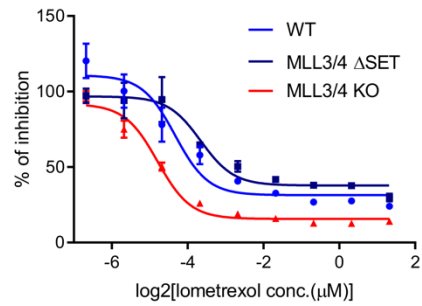
F Upregulated genes in MII3/4 WT only



G Upregulated genes in MII3/4 KO only

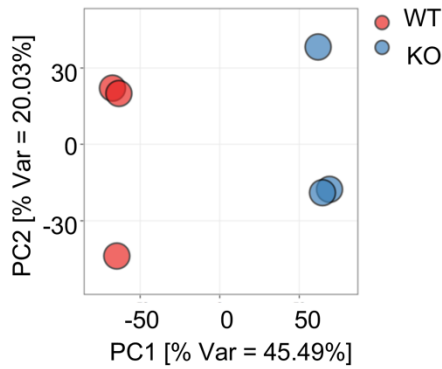


Supplemental Figure 4. MLL3/4 KO mESCs are more sensitive to purine synthesis inhibition. (A-B) WT and MLL3/4 KO cells were treated with 0 – 2.5 μ M lometrexol (LTX) (A) or 0 – 5 μ M methotrexate (MTX) (B) for 48 hours. A CellTiter-Glo® luminescent cell viability assay was performed to determine the percentage of cell growth inhibition under these conditions with three different MLL3/4 KO clones included. (C) WT and MLL3/4 KO cells were treated with 0 – 40 μ M SHIIN1 for 48 hours. An MTT cell viability assay was performed to determine the percentage of cell growth inhibition under these conditions with three different MLL3/4 KO clones included. n=3. (D) Venn diagram showing the overlap of genes upregulated upon LTX treatment in WT or KO cells. (E) Pathway enrichment analysis of the genes upregulated upon LTX treatment in both WT and KO cells. (F) Pathway enrichment analysis of the genes uniquely upregulated upon LTX treatment in WT cells. (G) Pathway enrichment analysis of the genes uniquely upregulated upon LTX treatment in MLL3/4 KO cells.

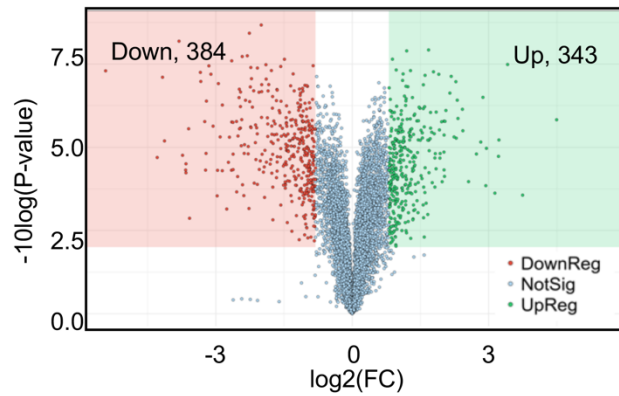
A**B****C**

Supplemental Figure 5. Loss of the MLL3/4 SET domain does not confer increased sensitivity to purine synthesis inhibition. (A) Western blot showing MLL4, MLL3, NCOA6, UTX, RbBP5 and ASH2L protein levels in WT, MLL3/4 Δ SET and MLL3/4 KO cells with Hsp90 as the loading control. Bulk levels of histone H3K4me1, H3K4me2, H3K4me3 and H3K27Ac are also shown. N, N-terminus; C, C-terminus. mESCs harboring deletion of the SET domains of both MLL3 and MLL4 (referred to as MLL3/4 Δ SET) were generated in our previous studies (3). (B) Western blot showing nuclear and cytoplasmic MLL4, UTX, NCOA6 and RBBP5 protein levels after cell fractionation, with MLL1 and Hsp90 serving as nuclear and cytoplasmic loading controls, respectively. (C) WT, MLL3/4 Δ SET and MLL3/4 KO cells were treated with 0 – 2.5 μ M lometrexol (LTX) for 72 hours. A CellTiter-Glo® luminescent cell viability assay was performed to determine the percentage of inhibition. n=2.

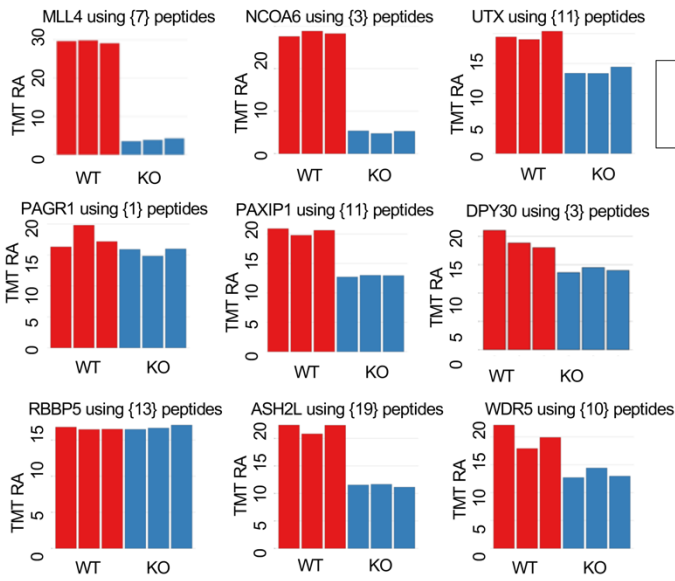
A PCA using all 7096 proteins



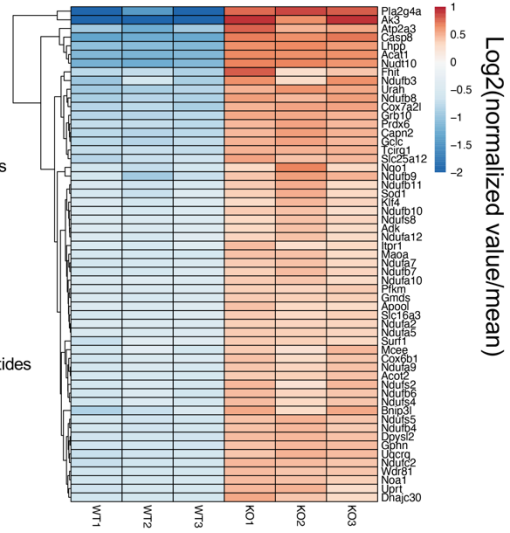
B



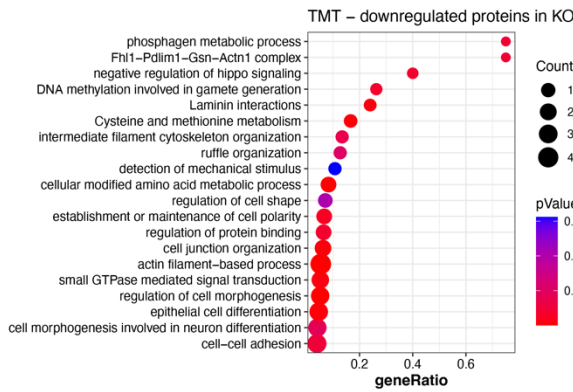
C



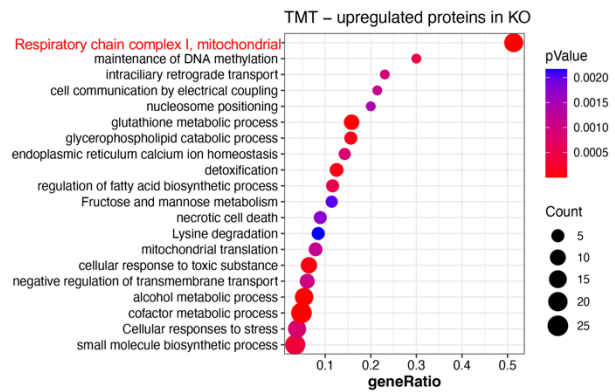
F 59 proteins in Group 1



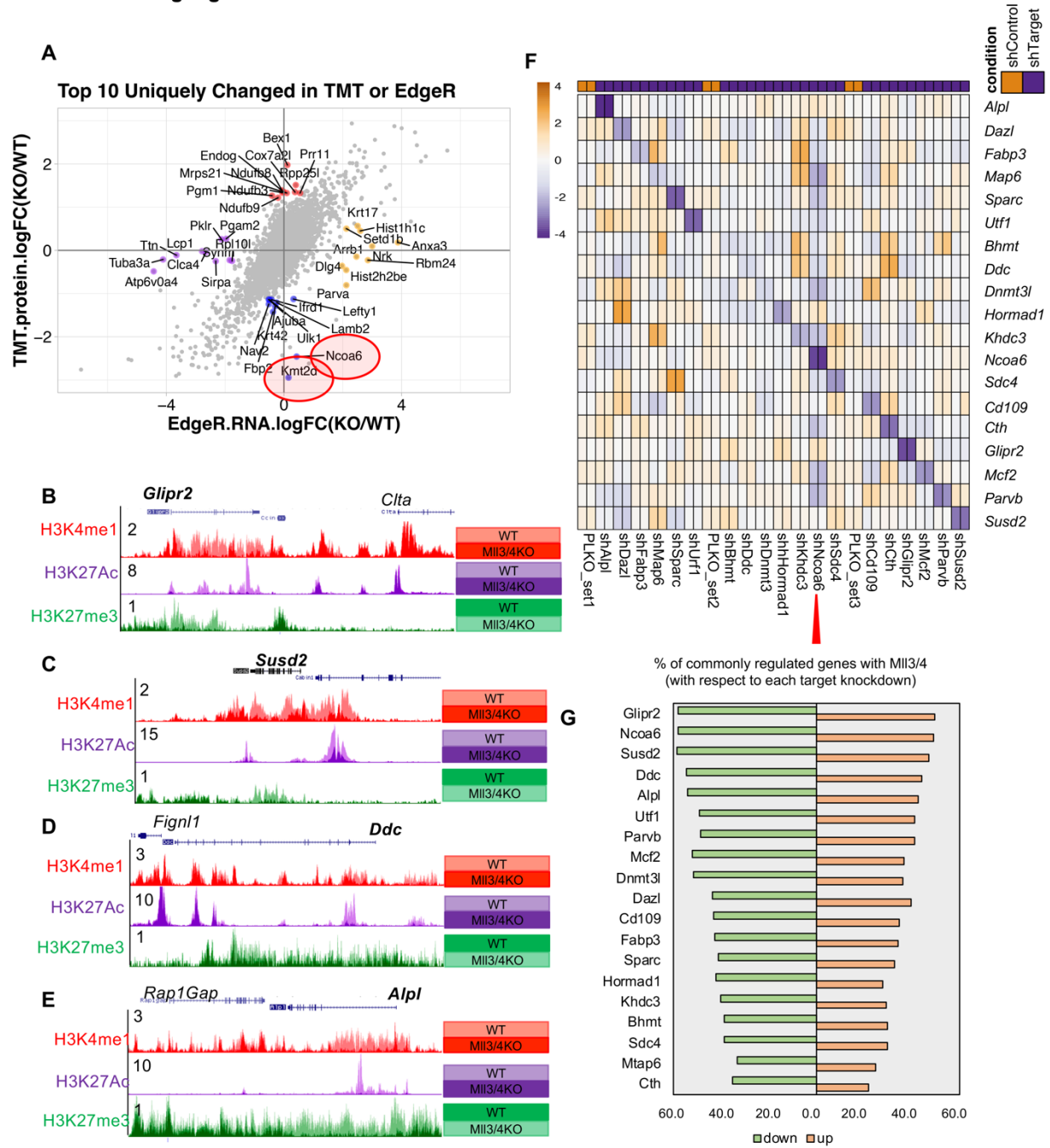
D



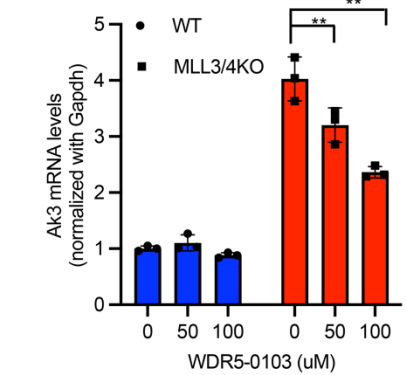
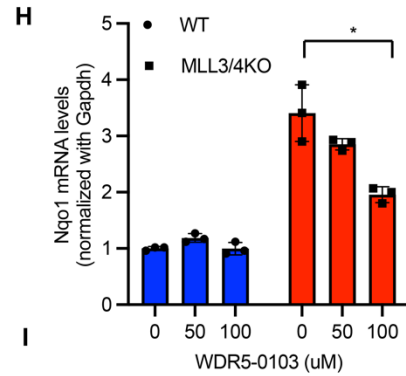
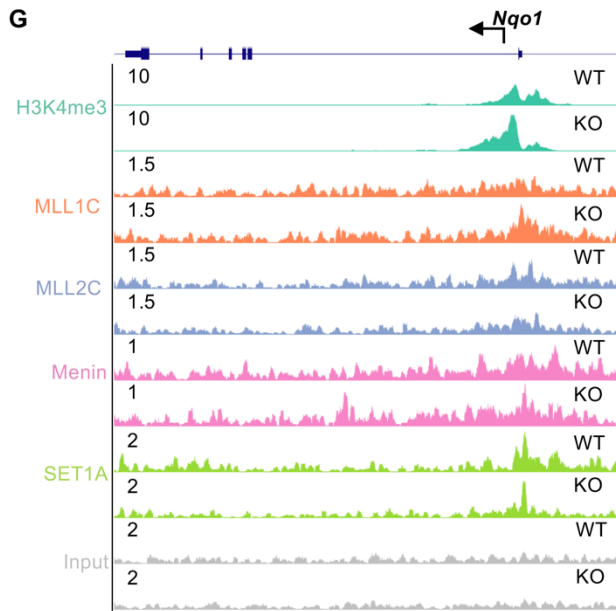
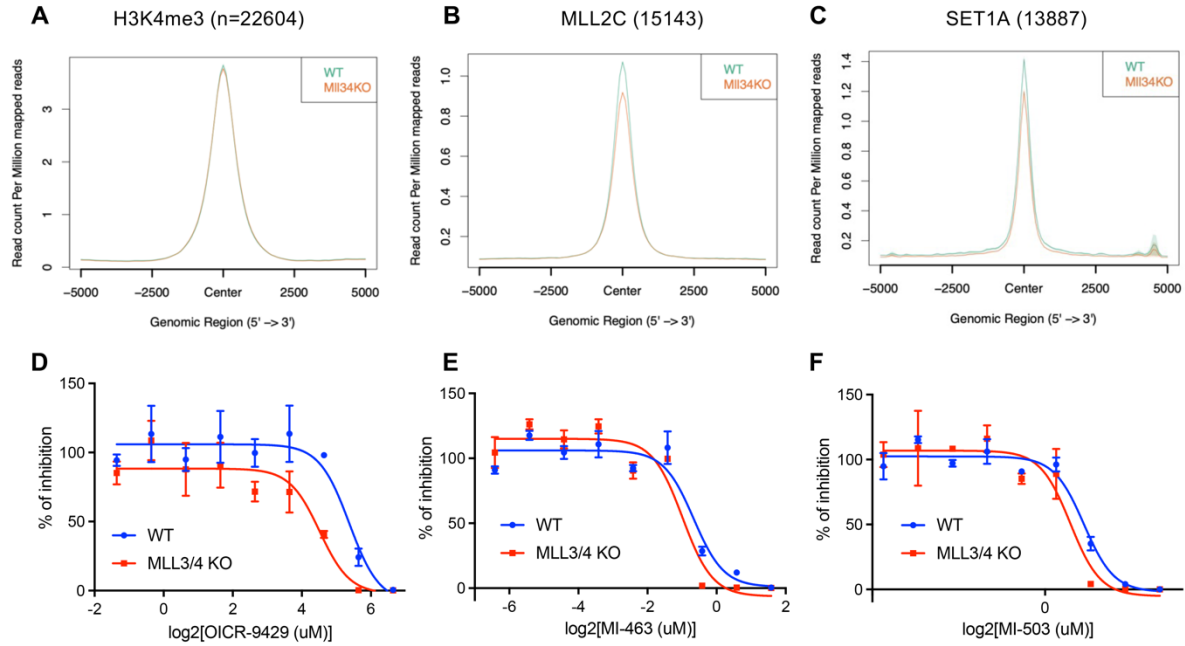
E



Supplemental Figure 6. TMT proteomics profiling identified purine metabolism upregulation in MLL3/4 KO cells. (A) TMT proteomics profiling was conducted in WT and MLL3/4 KO cells. PCA plot showing the separation of genotypes by PC1 using all 7096 proteins identified. (B) Volcano plot showing all the differentially abundant proteins in WT and KO cells with the cutoff $|FC| > 1.75$, $p.val < 0.01$. Up, 343 proteins; Down, 384 proteins. (C) Protein levels of MLL3/4 COMPASS subunits identified and quantified by the TMT approach. (D) Pathway enrichment analysis of the downregulated proteins in KO cells in comparison to WT cells. (E) Pathway enrichment analysis of the upregulated proteins in KO cells in comparison to WT cells. The mitochondrial respiratory chain complex I group (referred to as Group1 here) was significantly enriched. (F) Heatmap showing the 59 proteins in Group1 change in WT and KO cells related to nucleotide metabolic processes.

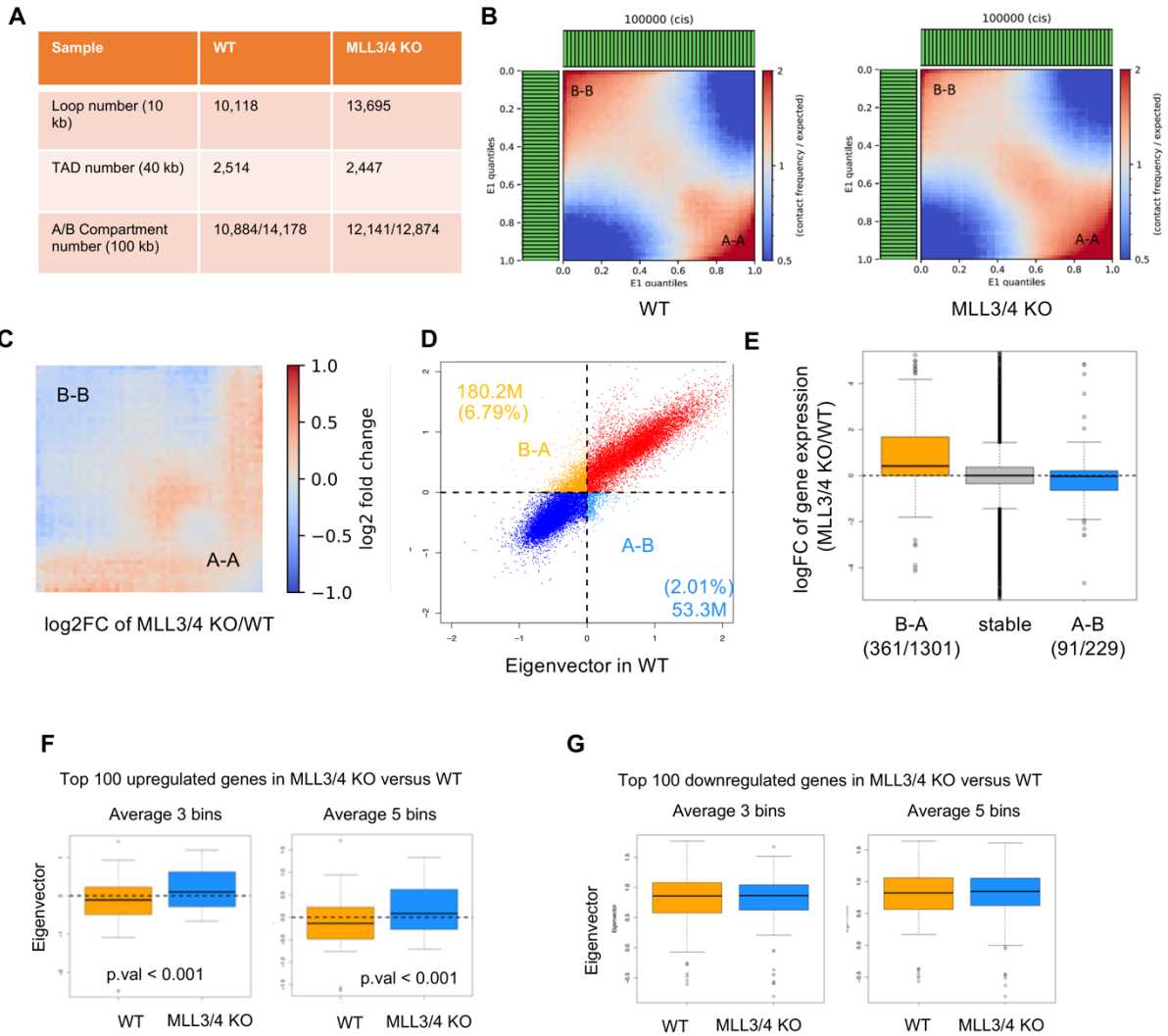


Supplemental Figure 7. RNA-seq and TMT proteomics profiling integration identified top MLL3/4 target genes. (A) The correlation analysis of TMT and EdgeR data identified factors including NCOA6 that were altered at the protein but not RNA levels. (B-E) Browser tracks with overlaid view of H3K4me1, H3K27Ac and H3K27me3 ChIP-seq for selected downregulated target genes including *Glipr2* (B), *Susd2* (C), *Ddc* (D), and *Alpl* (E). (F) Knockdown efficiency of each specific target shown by the z-score heatmap. (G) Percentage of genes regulated in common with MLL3/4 for each target knockdown.



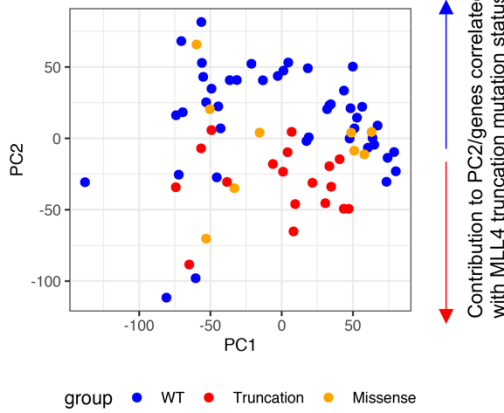
Supplemental Figure 8. MLL1 compensates the loss of MLL3/4 to activate gene expression.

(A) H3K4me3 ChIP-seq peaks in both WT and MLL3/4 KO cells were merged and sorted. Average plot showing the H3K4me3 signal in WT and MLL3/4 KO cells centered on all H3K4me3 peaks. n = 22604. (B) MLL2C (MLL2 Carboxyl-terminal antibody) ChIP-seq peaks in both WT and MLL3/4 KO cells were merged and sorted. Average plot showing the MLL2C signal in WT and MLL3/4 KO cells centered on all MLL2 peaks. n = 15143. (C) SET1A ChIP-seq peaks in both WT and MLL3/4 KO cells were merged and sorted. Average plot showing the SET1A signal in WT and MLL3/4 KO cells centered on all SET1A peaks. n = 13887. (D-F) Cell viability of WT and MLL3/4 KO cells in response to OIR-9429 (D), MI-463 (E) or MI-503 (F) treatment. N=3 for each specific concentration in WT and MLL3/4 KO. (G) ChIP-seq track showing the chromatin occupancy of H3K4me3, MLL1, MLL2, Menin and SET1A at the *Nqo1* gene locus in WT and MLL3/4 KO cells. (H) qRT-PCR showing *Nqo1* (H) and *Ak3* (I) gene expression in WT and MLL3/4 KO cells treated with 0, 50, or 100 μ M WDR5-0103. mRNA levels were normalized to the *Gapdh* internal control. Data are presented as mean \pm standard deviation (SD) with n=3. *P < 0.05, **P < 0.01 with unpaired t-test.

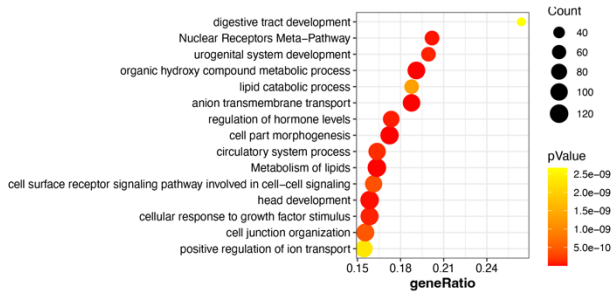


Supplementary Figure 9. Hi-C analysis in WT and MLL3/4 KO mESCs. (A) Loop number, TAD (Topologically Associated Domains) number, and A/B compartment occupancy numbers in WT and MLL3/4 KO mESCs. (B) Hi-C was performed in WT and MLL3/4 KO mESCs. Compartmentalization saddle plots of Hi-C data for WT and MLL3/4 KO ES cells, created using cooltools (4). Average intra-chromosomal interaction frequencies were normalized by expected interaction frequency and distance. Bins were sorted by eigenvector PC1 values. B-B interactions are located in the upper-left corner of saddle plots and A-A interactions are located in the lower-right corner. (C) Saddle plot of Log2FC of MLL3/4 KO versus WT. (D) A C-score was calculated for each 100-kb genomic bin to determine its A or B compartmentalization. Compartment switching, decompaction and compaction upon MLL3/4 loss are represented in the scatter plot. Lengths of genomic regions (no. of bins x 100 kb) and percentage of compartment shifts are shown. (E) Genes located in B-to-A shifted (B-A), stable and A-to-B shifted (A-B) bins were selected ($\geq \frac{1}{2}$ gene length located within the bins). 1301 and 229 genes were found in B-A and A-B group, respectively. Genes with detectable expression levels were further selected (361 for B-A and 91 for A-B) for analysis of the logFC gene expression in KO versus WT, shown in the box plot. (F-G) Eigenvector values for the top 100 up (F) or down (G) regulated genes. “3 bins average” is the average of the 100 kb bin containing the gene’s TSS and the two adjacent bins; “5 bins average” is the average of the 100 kb bin containing the gene’s TSS and the adjacent four bins.

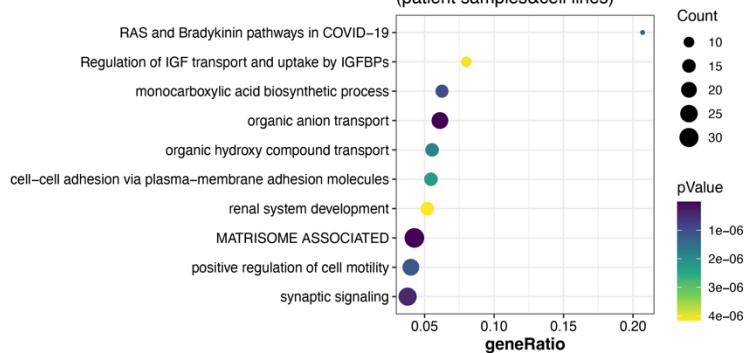
A CCLE colorectal cell lines (n = 71)
WT, 43; Truncation, 19; Missense only 9



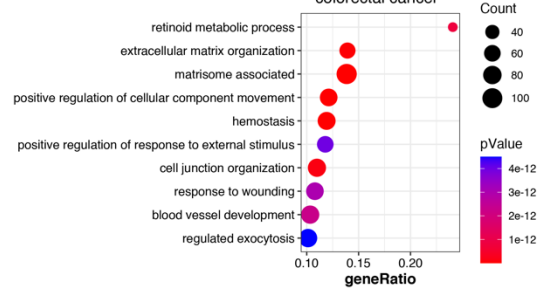
D Genes **downregulated** in MLL4 Truncation versus WT
(patient samples from TCGA PanCancer Atlas)



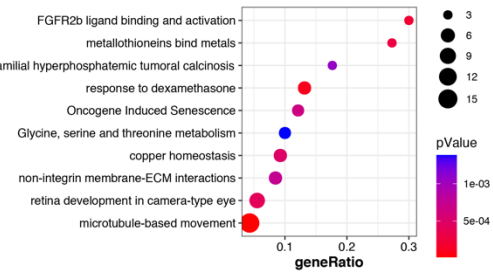
F genes downregulated in MLL4 Trunc.vs.WT
(patient samples&cell lines)



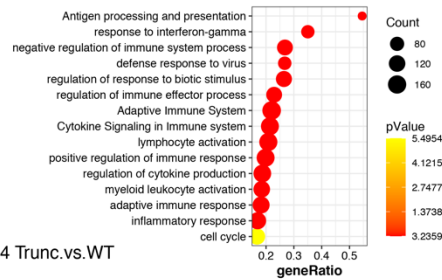
B pathways of downregulated genes
- MLL4 truncation versus WT
- colorectal cancer



C pathways of upregulated genes
- MLL4 truncation versus WT
- colorectal cancer



E Genes **upregulated** in MLL4 Truncation versus WT
(patient samples from TCGA PanCancer Atlas)

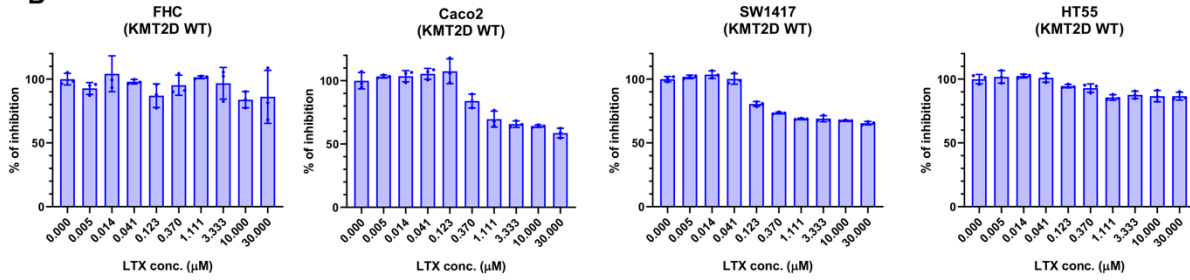


Supplemental Figure 10. Loss-of-function MLL4 mutations in colorectal cancer share similar gene expression features with mESC depleted of MLL3/4. (A) PCA of 71 colorectal cancer cell lines in the Cancer Cell Line Encyclopedia (CCLE) based on RNA-seq gene-expression data obtained from DepMap. Cell lines were grouped based on the MLL4 mutation status: WT, n= 43; Truncation, n = 19; Missense only, n = 9. If truncation mutation and missense mutation co-exist in one cell line, it is annotated as truncation. PC1, 24% variance; PC2, 11% variance. (B) Pathway analysis of genes downregulated in MLL4 truncation versus WT CCLE colorectal cancer cell lines. (C) Pathway analysis of genes upregulated in MLL4 truncation versus WT CCLE colorectal cancer cell lines. (D) Pathway analysis of genes downregulated in MLL4 truncation versus WT patient samples from the TCGA PanCancer Atlas. (E) Pathway analysis of genes upregulated in MLL4 truncation versus WT patient samples from the TCGA PanCancer Atlas. (F) Pathway analysis of genes downregulated in the MLL4 truncation versus WT condition in both CCLE colorectal cancer cell lines and patient samples from the TCGA PanCancer Atlas. Data were retrieved from cBioPortal with OQL (Onco Query language) to define MLL4 mutation status (<https://www.cbioportal.org/>).

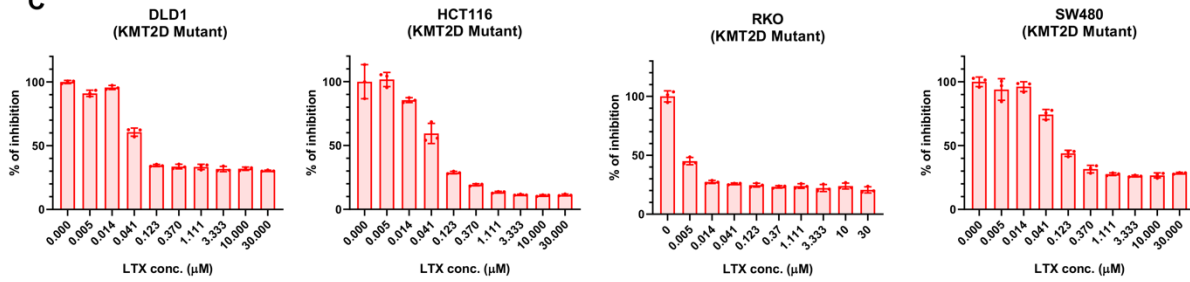
A

Cell Line	FHC, normal	Caco2	SW1417	HT55	SW480	DLD1	HCT116	RKO
KMT2D	-	WT	WT	WT	D1633N	F5284L, L2304M, P1931H, E1667D, E1517D	R2443Sfs*6, V160M	L5056P, G3465*, P2550Lfs*33, L1600P, R1189H
KMT2C	-	S2427G	S1416L, P2050L	G1584L	Q4279*	G3438D, I1706V	I1344*	R3853W
KDM6A	-	WT	WT	WT	WT	WT	WT	WT

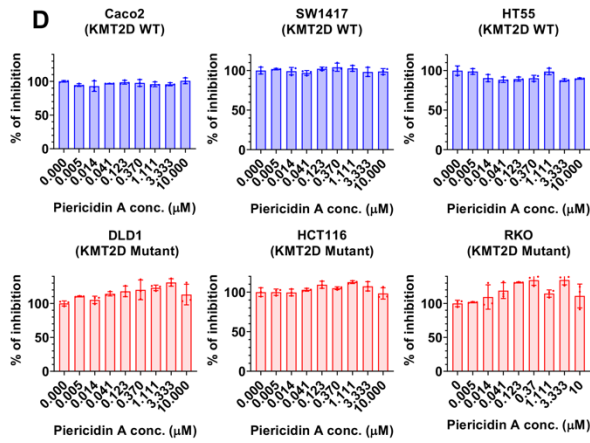
B



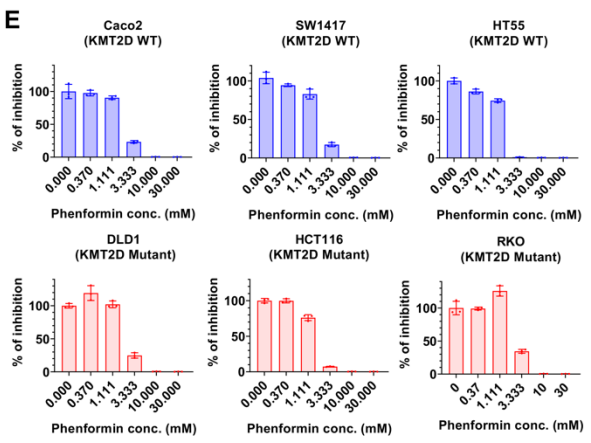
C



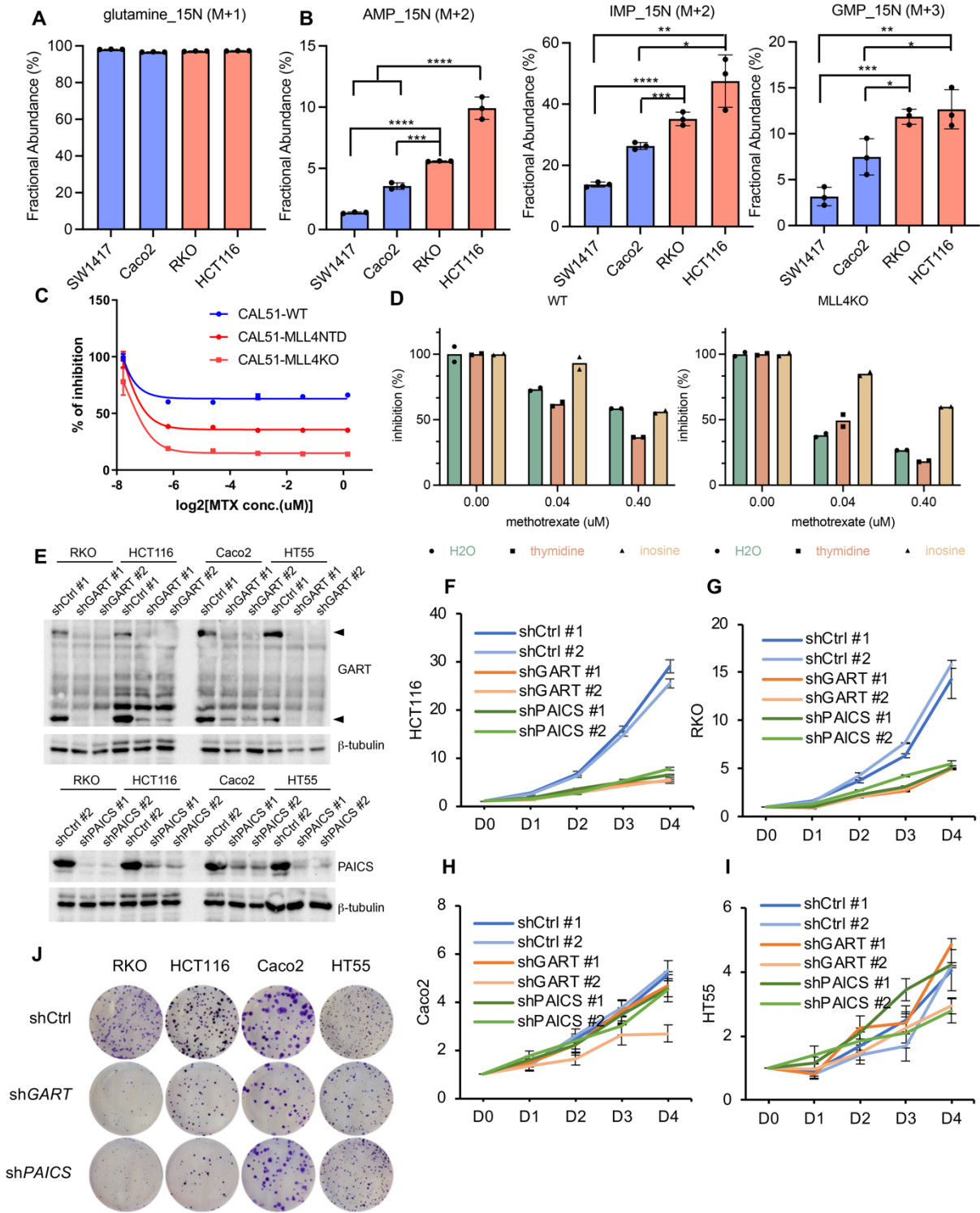
D



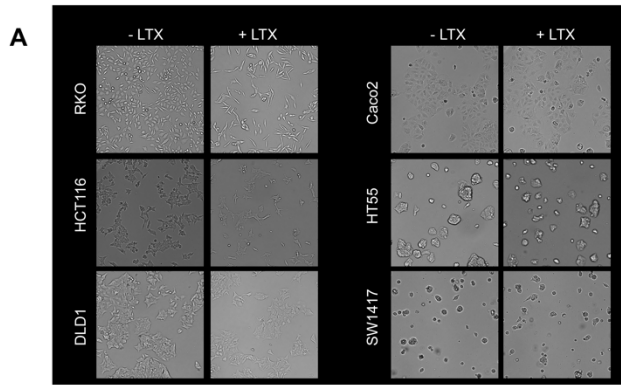
E



Supplemental Figure 11. MLL4 mutant colorectal cancer cells are selectively sensitive to lometrexol treatment. (A) MLL3/4 and UTX mutation status of the colorectal cell lines. (B-C) Cell growth inhibition upon LTX treatment (0 – 30 μ M) in MLL4 wild type (B) and MLL4 mutant (C) cell lines. (D-E) Cell growth inhibition upon treatment with Piericidin A (0 – 10 μ M) (D) or Phenformin (0 – 30 mM) (E) in MLL4 wild type and MLL4 mutant cell lines. CellTiter-Glo® luminescent cell viability assays were performed 72 hours after treatment to determine the percentage of inhibition under each treatment condition. Data are presented as mean \pm standard deviation (SD) with n=3. *P < 0.05, **P < 0.01, ***P < 0.001 with unpaired t-test.

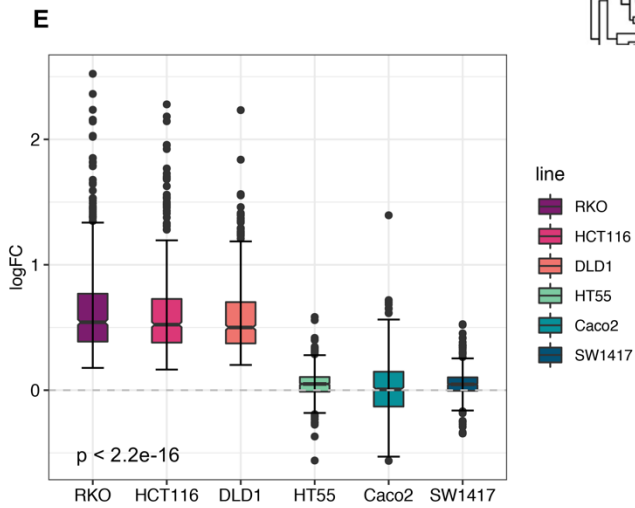
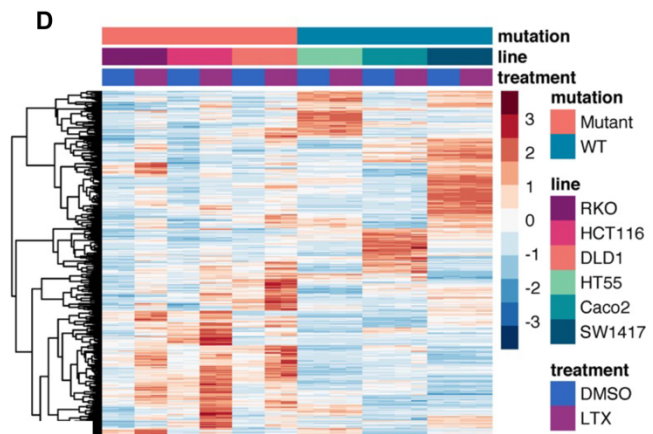
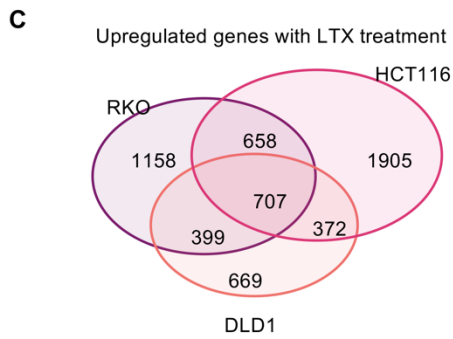


Supplemental Figure 12. Cells with compromised MLL4 function are selectively sensitive to de novo purine synthesis inhibition. (A) Tracer levels of glutamine (M+1) in SW1417, Caco2, RKO and HCT116 cells. (B) Incorporation of ¹⁵N tracer from glutamine into purines in SW1417, Caco2, RKO and HCT116 cells. MLL4 WT cells, blue; MLL4 mutant cells, red. Data are presented as mean ± standard deviation (SD) with n=3. *P < 0.05, **P < 0.01, ***P < 0.001, ****P < 0.0001 with unpaired t-test. (C) A CellTiter-Glo® luminescent cell viability assay was performed in CAL51 WT, heterozygous MLL4 truncation mutation (hNTD), and MLL4 KO cells treated with (MTX) (0 – 1 μM). n=3. (D) A CellTiter-Glo® luminescent cell viability assay was performed in CAL51 WT and MLL4 KO cells were treated with 0, 0.04, or 0.4 μM MTX in the presence of H₂O, 50 μM thymidine or 50 μM inosine. n=2. (E-J) Cells were infected with lentiviruses expressing shCtrl, shGART or shPAICS. Two distinct shRNAs were included for both GART and PAICS. Western blot showing the knockdown of GART and PAICS in RKO, HCT116, Caco2 and HT55 cells (E). The growth rates of HCT116 (F), RKO (G), Caco2 (H) and HT55 (I) cells with shCtrl, shGART or shPAICS were measured by cell counting (n=2), and the cell number was normalized to day 0. Colony formation in the four cell lines with GART or PAICS knockdown was performed by seeding 500 or 1000 cells in 6 well plates and staining after 10-14 days of culture with media changed every three days (J).



B

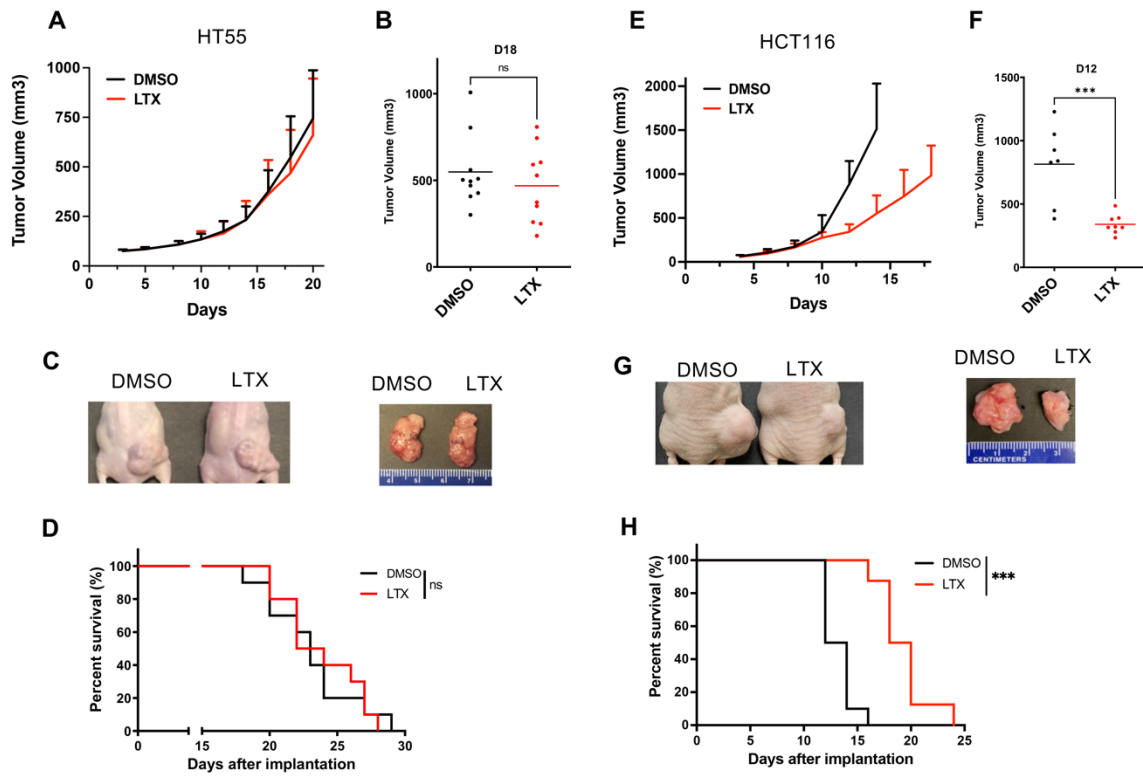
Line	KMT2D	direction	LTX_vs_DMSO
RKO	Mut	up	2922
RKO	Mut	dn	2980
HCT116	Mut	up	3642
HCT116	Mut	dn	3528
DLD1	Mut	up	2147
DLD1	Mut	dn	2096
HT55	WT	up	1
HT55	WT	dn	0
Caco2	WT	up	22
Caco2	WT	dn	3
SW1417	WT	up	91
SW1417	WT	dn	53



Commonly upregulated gene expression in LTX_vs_DMSO in RKO, HCT116, and DLD1 (n = 707)

Supplemental Figure 13. RNA-seq data in colorectal cancer cells treated with LTX. (A) Morphological change in colorectal cancer cell lines treated with LTX at 1 μ M for 24 hours viewed under bright field microscope. (B) summary of total differentially expressed gene numbers (up and down-regulated genes separated) in these cell lines, with MLL4 mutation status indicated. adj.p < 0.01. (C) Venn diagram showing the overlap of upregulated genes in LTX treated versus control in RKO, HCT116, and DLD1. (D) Hierarchical clustering heatmap showing the expression of genes upregulated in LTX treated versus control in common among RKO, HCT116 and DLD1 cell lines (n = 707). (E) Box plot showing the logFC of the 707 genes upregulated in common among RKO, HCT116 and DLD1 cells upon LTX treatment. An unpaired t-test was used to calculate the p value. Gene expression was significantly different compared with MLL4 WT cells for all the MLL4 mutant cell lines.

Supplemental Figure 14. The unique gene expression signature of MLL4 mutant cells in response to LTX treatment. (A-B) RNA-seq track examples showing the AURKA (A) and PLK1 (B) gene expression in MLL 4 mutant (DLD1, HCT116, RKO) or WT (SW1417, Caco2, HT55) colorectal cancer cell lines in response to LTX treatment. (C) A collection of 217 genes related to mitotic cell cycle pathways was selected for visualization. Volcano plots highlighting the top 20 downregulated genes involved in mitotic cell cycle pathways in MLL4 mutant cell lines (RKO, HCT116 and DLD1). The 10 genes found in common among the plots (PLK1, AURKA, CDCA3, CDC20, SFPQ, POLA1, PSRC1, KIF20A, FAM83D, and DLGAP5) were defined as the “lometrexol responsive mitotic gene signature” (D) Volcano plots showing the expression of these 10 genes in MLL4 WT cell lines (HT55, Caco2 and SW1417).



Supplemental Figure 15. Lometrexol application in MLL4 mutant tumors in the xenograft mouse models. (A-D) Tumor development after inoculation of 4×10^6 of HT55 cells into nude mice. Mice with HT55 subcutaneous (sc) tumors were treated with either vehicle (DMSO, n = 9) or LTX (15 mg/kg, n = 9) daily for 7 days. (A) Growth plots for sc tumors in each treatment group are shown with mean tumor volumes (mm^3 and upper SD). (B) Dot plot representation of sc tumor volume in mice at day 18 post-tumor cell injection. Unpaired t-test values for comparisons between DMSO and LTX treatment: ns, not statistically significant. (C) Photographs of nude mice (left) in which HT55 cells were inoculated into the right flank and sc tumors taken from these mice (right). (D) Animal survival at the indicated days after inoculation. Log-rank test was used for comparisons between DMSO and LTX treatment. (E-H) Tumor development after inoculation of 4×10^6 of HCT116 cells into nude mice. Mice with HCT116 subcutaneous (sc) tumors were treated with either vehicle (DMSO, n = 9) or LTX (15 mg/kg, n = 9) daily for 7 days. (E) Growth plots for sc tumors in each treatment group are shown with mean tumor volumes (mm^3) and upper SD. (F) Dot plot representation of sc tumor volume in mice at day 12 post-tumor cell injection. Unpaired t-test values for comparisons between DMSO and LTX treatment: ***, $P < 0.001$. (G) Photographs of nude mice (left) in which HCT116 cells were inoculated into the right flank and sc tumors taken from these mice (right). (H) Animal survival at the indicated days after inoculation. Log-rank test was used for comparisons between DMSO and LTX treatment: ***, $P < 0.001$.

Table S1.

Mouse shRNA					
Clone ID	Oligo Seq	Symbol	RefSeq ID	Gene ID	Gene Description
TRCN0000081503	CCGGGCAGGAACAGAAGTTCGCTATCTCGAGATAGCGAACTTCTGTTCCCTGCTTTTTG	Alpl	NM_007431	11647	alkaline phosphatase 2, liver
TRCN0000080349	CCGGCCTAGACAACGACAAGTACATCTCGAGATGTACTTGTCTGTTCTAGGTTTTG	Sparc	NM_009242	20692	secreted acidic cysteine rich glycoprotein
TRCN0000081712	CCGGCTTCGACCAAACCGTTTCTCTCTCGAGAGAGAAACGGTTTGGTCTGAAGTTTTG	Utf1	NM_009482	22286	undifferentiated embryonic cell transcription factor 1
TRCN0000102500	CCGGGCCTTGTGATCTATCTTGTACTCGAGTACAAGATAGATCAACAAGGCTTTTTG	Dazl	NM_010021	13164	deleted in azoospermia-like
TRCN0000105190	CCGGGCCTACTACCATCATCGAGAAGTCTCGAGTTCTCGATGATGGTAGTAGGCTTTTTG	Fabp3	NM_010174	14077	fatty acid binding protein 3, muscle and heart
TRCN0000340859	CCGGAGCAAGCACTAAGGATCAAAGCTCGAGCTTTGATCCCTTAGTGCTTCTTTTTG	Map6	NM_010837	17760	microtubule-associated protein 6
TRCN0000331554	CCGGGATTCGAGAGACAGAGGTCATCTCGAGATGACCTCTGTCTCTCGAATCTTTTTG	Sdc4	NM_011521	20971	syndecan 4
TRCN0000097583	CCGGCGCTTAAATGCCGGAGAAGTCTCGAGAAGTCTCCGGCATTTAAGCGTTTTG	Bhmt	NM_016668	12116	betaine-homocysteine methyltransferase
TRCN0000108475	CCGGGCCTTTAATATGGACCCTGTTCTCGAGAACAGGGTCCATATTAAGGCTTTTTG	Ddc	NM_016672	13195	dopa decarboxylase
TRCN0000039105	CCGGCTTCTGGATATTCATGGACAAGTCTCGAGTTGTCCATGAATATCCAGAAGTTTTG	Dnmt3l	NM_019448	54427	DNA (cytosine-5-)-methyltransferase 3-like
TRCN0000173430	CCGGCCTAGAGTACAGGGTGAACATCTCGAGATGTTCAACCTGTACTCTAGGTTTTG	Ncoa6	NM_019825	56406	nuclear receptor coactivator 6
TRCN0000446257	CCGGGCGAGCTGAGATTTGGATATCTCGAGATATCCAAATCTCAGCTCGCCTTTTTG	Khdc3	NM_025890	66991	RIKEN cDNA 2410004A20 gene
TRCN0000200876	CCGGGAAGAGAAGTCTTCGTCAATTCTCGAGAATTGACGAGACTTCTCTTTTTG	Hormad1	NM_026489	67981	HORMA domain containing 1
TRCN0000110910	CCGGCGCTAATTTGATCCTGTGTTTCTCGAGAAACACAGGATCAAATTAGCGTTTTG	Glipr2	NM_027450	384009	GLI pathogenesis-related 2
TRCN0000126003	CCGGCGAGACCCATTGGCAATACTACTCGAGTAGTATTGCCAATGGGTCTCGTTTTG	Susd2	NM_027890	71733	sushi domain containing 2
TRCN0000112644	CCGGCGGGACGCCTTCGATACTTCTCTCGAGAAGAGTATCGAAGCGTCCCGTTTTG	Parvb	NM_133167	170736	parvin, beta

TRCN00000 42657	CCGGGCTGACATACATTGATGACAACTCGAGTTGTCATCA ATGTATGTCAGCTTTTTG	Mcf2	NM_13 3197	109904	mcf.2 transformin g sequence
TRCN00004 20527	CCGGCACCTTCATGTCTGCATATTTCTCGAGAAATATGCAG ACATGAAGGTGTTTTTG	Cth	NM_14 5953	107869	cystathiona se (cystathioni ne gamma- lyase)
TRCN00000 80513	CCGGCCAGTGATGCTGTAAGTCATTCTCGAGAATGACTTA CAGCATCACTGGTTTTG	Cd10 9	NM_15 3098	235505	CD109 antigen
Human shRNA					
Clone ID	Target Sequence	Symb ol	RefSeq ID	Gene ID	Gene Description
TRCN00002 89428	CCCTAACTGTTGTCATGGCAA	GART #1	NM_00 0819	2618	AIRS, GARS, GARTF, PAIS, PGFT, PRGS
TRCN00002 89431	GCACAGTCTCATCATGTCAA	GART #2	NM_00 0819	2618	AIRS, GARS, GARTF, PAIS, PGFT, PRGS
TRCN00000 45774	CGCAGTGTGAAATGATTCCAA	PAIC S #1	NM_00 6452	10606	ADE2, ADE2H1, AIRC, PAIS
TRCN00000 45775	GCTGCTCAGATATTTGGGTTA	PAIC S #2	NM_00 6452	10606	ADE2, ADE2H1, AIRC, PAIS
qRT-PCR primers					
Ak3-QF	GCCTGAAGGGATGTGGTATTAG				
Ak3-QR	CCTGTTAAGGTAGCAGTGAGTT				
Nqo1-QF	GAGAAGAGCCCTGATTGACTG				
Nqo1-QR	ACCTCCCATCCTCTCTTCTT				
Gapdh-QF	AACAGCAACTCCCACTCTTC				
Gapdh-QR	CCTGTTGCTGTAGCCGTATT				

References

1. K. Cao *et al.*, An MLL4/COMPASS-Lsd1 epigenetic axis governs enhancer function and pluripotency transition in embryonic stem cells. *Sci Adv* **4**, eaap8747 (2018).
2. G. Yu, L. G. Wang, Q. Y. He, ChIPseeker: an R/Bioconductor package for ChIP peak annotation, comparison and visualization. *Bioinformatics* **31**, 2382-2383 (2015).
3. R. Rickels *et al.*, Histone H3K4 monomethylation catalyzed by Trr and mammalian COMPASS-like proteins at enhancers is dispensable for development and viability. *Nat Genet* **49**, 1647-1653 (2017).
4. J. H. Gibcus *et al.*, A pathway for mitotic chromosome formation. *Science* **359**, (2018).